AIAA JOURNAL
Vol. 36, No. 6, June 1998

Evaluation of Reynolds Stress Closure for Turbulent Boundary Layer in Turbulent Freestream

J. C. Mackinnon,* M. Renksizbulut,† and A. B. Strong‡
University of Waterloo, Waterloo, Ontario N2L 3G1, Canada

Calculations for the interaction of grid-generated freestream turbulence with a turbulent boundary layer using the Gibson–Launder Reynolds stress model are presented. Based on detailed comparisons to experimental data, it is found that the Gibson–Launder model in general gives good predictions of friction drag and momentum and displacement thicknesses, but not of the boundary-layer thickness. Experimentally observed trends in turbulent and mean profiles as a function of the freestream turbulence intensity and the ratio of the free-stream length scale to the boundary-layer thickness are also generally well predicted. It is identified, however, that the Gibson–Launder model does not properly account for the effect of the wall, resulting in the normal turbulent stress being attenuated at too great a distance from the wall. It is also observed that, when the conventional gradient diffusion model is used for third-order correlations, the calculations underpredict experimental results and the contribution of turbulent diffusion. Implementation of improved formulations for both turbulent diffusion modeling and the wall-reflection term in the pressure-strain model result in improved predictions of experimental data.

Nomenclature

C_f = friction drag coefficient
C_{ijk} = convection of $\overline{u_i u_j u_k}$
D_{ijk} = diffusion of $\overline{u_i u_j u_k}$
f = length scale function in the wall-reflection term
I_∞ = freestream turbulence intensity
k = turbulent kinetic energy per unit mass
L_u^∞ = longitudinal dissipation length scale
L_{ue} = freestream longitudinal integral length scale
M = mesh width of turbulence generating grid
P_z = production of turbulent quantity z
$\bar{P}, p$ = mean and fluctuating pressure
p_r = length scale ratio, L_u^∞ / L_{ue}
Re_θ = Reynolds number based on momentum thickness
U_{def} = velocity defect, $[\bar{U}_\infty - \bar{U}(y)]/U_\tau$
U_τ = friction velocity, $(\tau_w/\rho)^{1/2}$
$\bar{U}, \bar{V}$ = mean velocity in x and y directions, respectively
$\overline{u_i u_j u_k}$ = third-order correlation between fluctuating components
$\overline{uv}$ = turbulent shear stress
$\overline{u^2}, \overline{v^2}, \overline{w^2}$ = turbulent stresses in x, y, z directions, respectively
v^{2*} = nondimensional stress, $\overline{v^2}/v_\infty^2$
W = wall-reflection term
y^* = nondimensional position, y/L_{ue}
α_1, α_2 = nondimensional freestream values of $\overline{u^2}$, $\overline{v^2}$, respectively
β = freestream turbulence parameter, $I_\infty/(2 + L_u^\infty/\delta)$
δ = mean boundary-layer thickness at $0.995\bar{U}_\infty$
δ_{ij} = Kronecker delta
δ^* = displacement thickness
ϵ = isotropic dissipation rate of k per unit mass
ϵ_{ijk} = dissipation rate of $\overline{u_i u_j u_k}$
θ = momentum thickness
κ = von Kármán constant
ν = kinematic viscosity
Π_{ij} = pressure-strain correlation
ρ = density
τ_w = wall shear stress
ϕ_{ijk} = pressure interaction term in the $\overline{u_i u_j u_k}$ equation

Subscripts and Superscripts

calc = calculated
exp = experimental
n = direction normal to the wall
∞ = freestream value
$+$ = log-law coordinates
$*$ = nondimensionalized by freestream value

Received Aug. 12, 1997; revision received Jan. 5, 1998; accepted for publication Jan. 27, 1998.

*Graduate Student, Mechanical Engineering Department; currently Senior Design Engineer, Thermal Hydraulic Analysis Department, Ontario Hydro, 700 University Avenue, Toronto, Ontario M5G 1X6, Canada.
†Professor, Mechanical Engineering Department. Senior Member AIAA.
‡Professor Emeritus, Mechanical Engineering Department.

I. Introduction

THE interaction of an external turbulent flow with an underlying boundary layer is a complex flow commonly encountered in many engineering problems, ranging from simple heat exchangers to complex turbomachinery. Experimental studies of such flows have shown that the presence of freestream turbulence substantially affects both the momentum and heat transfer in the boundary layer formed on surfaces. Because the design of such equipment involves computer codes with turbulence models for the associated fluid dynamics and heat transfer, there is a need for accurate calculations.

The physical phenomena in these problems are complex. For example, for the highly turbulent gas flow over turbine blades, they include boundary-layer transition, pressure gradient and streamline curvature due to the blade geometry, and freestream turbulence. The interaction of a turbulent freestream with a turbulent boundary layer formed on a flat plate is a relatively simpler flow that retains important features of more complicated flows and, as such, allows for a methodology to be established by which turbulence model components may be evaluated and developed in reasonable isolation. Calculations for this flow are the focus of the present work.

Experimental investigations primarily address the interaction between decaying grid-generated turbulence and the boundary layer formed on a solid flat plate. For negligible or zero pressure gradient flows, with Reynolds number based on momentum thickness greater than approximately 2000, the effect of the freestream on boundary-layer structure is determined by the turbulence intensity I_∞ and the ratio of a typical freestream length scale L_u^∞ to the boundary-layer thickness δ (Refs. 1–3):

$$L_u^\infty = \frac{-\left(\overline{u_\infty^2}\right)^{\frac{3}{2}}}{\bar{U}_\infty\left(\mathrm{d}\overline{u_\infty^2}/\mathrm{d}x\right)}, \qquad I_\infty = \frac{\sqrt{\overline{u_\infty^2}}}{\bar{U}_\infty} \tag{1}$$

Through detailed measurements taken over a range of L_u^∞/δ (0.7–5) and I_∞ (0–6%), Hancock[3] (also reported in Refs. 4 and 5)

assessed the independent effects of these parameters on boundary-layer characteristics. Subsequent experiments by Baskaran et al.[6] and Hoffmann and Mohammadi[7] have further increased the database.

In general, freestream turbulence thickens the boundary layer and increases its growth rate relative to that with a laminar freestream. An increase in I_∞ increases this interaction and, hence, C_f. The importance of L_u^∞ may partially be explained by considering the impermeability of a solid boundary. Hancock's experiments indicate that the maximum effect of the freestream on the boundary layer is found when $L_u^\infty/\delta \sim 1$. As the length scale ratio increases, the effect of the freestream is reduced due to an attenuation in the fluctuations normal to the wall at the edge of the boundary layer.

A number of numerical studies have also been performed. McDonald and Kreskovsky[8] and Blair and Edwards[9] solved the momentum boundary-layer equations by employing an eddy viscosity formulation in conjunction with an integral form of the k equation. The limited data used in comparisons did not allow the separate effect of changes in L_u^∞/δ and I_∞ on the boundary-layer structure to be considered. At the 1980–1981 Stanford Conference, attempts were made to predict an empirical relationship for the change in the friction coefficient ΔC_f relative to that with a laminar freestream $C_{f,0}$ as a function of the parameter $\beta = I_\infty/(2 + L_u^\infty/\delta)$ (Ref. 10). Numerical solutions using an integral model, a k–ϵ formulation, and an algebraic stress model (ASM) were submitted. With the exception of the integral model, all calculations underpredicted the correlation. None of the models could properly account for the effects of the freestream length scale. The same general conclusions were also reached by Savill[11] using an ASM. More recently, Shima,[12] using a low Reynolds number second-moment closure based on the widely used high Reynolds number formulation of Gibson and Launder,[13] presented good predictions of the $\Delta C_f/C_{f,0}$ relationship. The improved predictions relative to those obtained in other studies were attributed to the modified formulation of the dissipation rate equation.

Using both a k–ϵ model and the Gibson–Launder[13] Reynolds stress model, as well as Hancock's[3] data for comparison, Rodi and Scheurer[14] have performed the most complete numerical study of this problem. They concluded from predictions of the $\Delta C_f/C_{f,0}$ relationship that the effect of length scale ratio was opposite to that observed in the experiments. The wall shear stress was generally well predicted by both models, but at large L_u^∞/δ, the velocity profile was predicted to be too full. The k profile was underpredicted by both models, which was attributed to the underprediction of the diffusion contribution to the kinetic energy balance, particularly in the outer portion of the boundary layer. Overall, the Reynolds stress closure gave better agreement with the data. Rodi and Scheurer concluded that the gradient diffusion assumption used in the turbulent diffusion models may not be valid for freestream turbulence and that the difficulty of capturing the length scale effects in the Reynolds stress model was partially due to the modeling of the attenuation of $\overline{v^2}$ by the wall.

Previous numerical studies have not provided a complete assessment of any turbulence model's ability to capture the effect of freestream turbulence on boundary-layer structure; the separate effects of L_u^∞/δ and I_∞ have not been isolated. In addition, an evaluation of predictions of the layer thicknesses (δ, δ^*, θ), turbulent normal stresses, and third-order correlations has not been carried out. In this paper, a methodology is presented to perform a thorough validation of turbulence models for this flow, both in the experimental conditions to examine and the requirements to be met by any model. Calculations are performed with the widely used Gibson–Launder high Reynolds number formulation. Weaknesses in the model (turbulent diffusion and wall reflection) previously identified in the literature are confirmed here, and new formulations for these models are presented and shown to give improved predictions.

II. Selection of Experimental Data for Validation

The experimental study used in assessing model predictions should ideally 1) have measurements of local, mean, and turbulent quantities in both the boundary layer and the free-stream; 2) be conducted over a wide range of conditions with the effects of I_∞ and L_u^∞/δ isolated; 3) have no other complicating phenomena present, e.g., low Reynolds number; 4) have measurements reported at many stations along the length of the plate; and 5) report uncertainty of all variables. An assessment of the suitability of available data is given in Mackinnon[15] and Hancock[3]; most are not appropriate for comparative purposes due to deficiencies in meeting the listed criteria. The most detailed studies are discussed here. Experiments of Charnay et al.[16] did not clearly distinguish the effects of I_∞ and L_u^∞/δ, and measurements were taken at only one station. In the study of Blair and Edwards,[9] only a limited range of experimental conditions was investigated, with no information available to establish the separate effect of L_u^∞/δ on boundary-layer characteristics. For the present investigation, Hancock's[3] measurements are used because his work comes closest to meeting all of the listed criteria. Confidence in Hancock's results is established by agreement with those of other researchers (data obtained prior to 1980, and in more recent studies indicated in the Introduction).

Hancock[3] conducted 13 experiments, four with a laminar freestream (LFS), denoted LFS1–LFS4 here, and nine with a turbulent freestream (TFS), denoted TFS1–TFS9. Local parameters and mean velocity profiles at multiple x locations are available in runs LFS3, LFS4, TFS1, TFS2, TFS3, TFS8, and TFS9; turbulent profiles were measured at multiple x locations only for runs LFS4, TFS2, and TFS9. In the presentation of results here, a station number may be appended as necessary, such as TFS9s12, where the x location of a given station in meters is related to its number N by the relationship $x = 0.152N$. Freestream turbulence was generated by placing grids upstream of the leading edge of the plate. Roughness at the start of the plate was used to trip the boundary layer. Heating wires were also used in some experiments, allowing for conditional sampling through slight heating of the boundary-layer fluid. The measurements were performed using hot-wire anemometry.

Hancock[3] did not report experimental uncertainty for all quantities. Bradshaw[10] reported the uncertainties in C_f and $\bar{U}(y)/\bar{U}_\infty$ for the experiments as 2% and less than 1%, respectively. Typical reported errors for local quantities,[1,2,17] for use only as a guideline, are 2% for C_f, 5% for δ, 4% for δ^*, and 1.5% for θ. For time-averaged turbulence quantities, Johnston and Flack[18] report that uncertainties in the normal and shear stresses of 5 and 10%, respectively, are attainable using a hot-wire X-probe. For third-order correlations, they are likely not much different than for double correlations.[18]

III. Mathematical Model and Numerical Solution

Steady, two-dimensional, high Reynolds number, incompressible, and constant property flows over a flat plate are considered here. For the boundary layer, the thin shear layer forms of the governing equations (demonstrated by Hancock[3] to be appropriate in the presence of freestream turbulence) are used. The continuity and x-momentum equations are

$$\frac{\partial \bar{U}}{\partial x} + \frac{\partial \bar{V}}{\partial y} = 0 \tag{2}$$

$$\frac{\mathrm{D}\bar{U}}{\mathrm{D}t} = -\frac{\partial(\overline{uv})}{\partial y} - \frac{1}{\rho}\frac{\partial \bar{P}}{\partial x} \tag{3}$$

The pressure gradient term is included here to account for the slight freestream acceleration observed in the experiments.

The conservation equation for a Reynolds stress $\overline{u_i u_j}$ has the form

$$\frac{\mathrm{D}\overline{u_i u_j}}{\mathrm{D}t} = -\left(\frac{\partial}{\partial x_k}\overline{u_i u_j u_k} + \frac{\overline{pu_j}}{\rho}\delta_{ik} + \frac{\overline{pu_i}}{\rho}\delta_{jk} - \nu\frac{\partial \overline{u_i u_j}}{\partial x_k}\right) - \left(\overline{u_i u_k}\frac{\partial \bar{U}_j}{\partial x_k} + \overline{u_j u_k}\frac{\partial \bar{U}_i}{\partial x_k}\right) - 2\nu\overline{\frac{\partial u_i}{\partial x_k}\frac{\partial u_j}{\partial x_k}} + \overline{\frac{p}{\rho}\left(\frac{\partial u_i}{\partial x_j} + \frac{\partial u_j}{\partial x_i}\right)} \tag{4}$$

representing convection, diffusion, production, dissipation, and pressure strain, respectively.

The basis of the present work is the widely used Gibson–Launder[13] high Reynolds number closure model (GLM). The GLM continues to be a basis for much high Reynolds number and near-wall modeling.[12,19] Further, near-wall models are being developed

that use the GLM as the high Reynolds number asymptote.[19] As such, it was appropriate to subject this model to rigorous testing against experimental data and to use it as a basis for further development.

Dissipation is distributed equally among the normal stresses, and the diffusion term is modeled through the gradient diffusion formulation of Daly and Harlow[20]:

$$-\frac{\partial \overline{u_i u_j u_k}}{\partial x_k} = \frac{\partial}{\partial x_k}\left(c_s \frac{k}{\epsilon}\overline{u_k u_l}\frac{\partial \overline{u_i u_j}}{\partial x_l}\right) \tag{5}$$

The pressure-strain correlation Π_{ij} is expressed as

$$\Pi_{ij} = \Pi_{ij,1} + \Pi_{ij,2} + \Pi_{ij,3} \tag{6}$$

Models of $\Pi_{ij,1}$ and $\Pi_{ij,2}$ are based on isotropization of stresses and mean production

$$\Pi_{ij,1} = -c_1(\epsilon/k)\left(\overline{u_i u_j} - \tfrac{2}{3}k\delta_{ij}\right), \qquad \Pi_{ij,2} = -c_2\left(P_{ij} - \tfrac{2}{3}P_k\delta_{ij}\right) \tag{7}$$

Because $\Pi_{ij,3}$ is a surface integral that accounts for the effect of a solid boundary in modifying the fluctuating pressure field, it is referred to as the wall-reflection term,

$$\Pi_{ij,3} = f c_1'(\epsilon/k)\left(\overline{u^2}_n\delta_{ij} - \tfrac{3}{2}\overline{u_n u_i}\delta_{nj} - \tfrac{3}{2}\overline{u_n u_j}\delta_{ni}\right) + f c_2'\left(\Pi_{nn,2}\delta_{ij} - \tfrac{3}{2}\Pi_{ni,2}\delta_{nj} - \tfrac{3}{2}\Pi_{nj,2}\delta_{ni}\right) \tag{8}$$

The effect of the turbulent length scale l, typically taken as being proportional to $k^{1.5}/\epsilon$, is accounted for through the linear length scale function $f(l/x_n)$. If l increases at a given y location, the magnitude of the wall-reflection term should also increase.

To close the equation set, ϵ is evaluated using[21]

$$\frac{\partial \bar{U}\epsilon}{\partial x} + \frac{\partial \bar{V}\epsilon}{\partial y} = \frac{\partial}{\partial y}\left(c_\epsilon \overline{v^2}\frac{k}{\epsilon}\frac{\partial \epsilon}{\partial y}\right) + c_{\epsilon 1}\frac{\epsilon}{k}P_k - c_{\epsilon 2}\frac{\epsilon^2}{k} \tag{9}$$

The wall function treatment employed in solving the governing equations in the near-wall log-law region is described by Rodi and Scheurer,[14] and the details of its application in the present work are given in Ref. 15. Bradshaw[10,22] indicates that the log-law region would be recognizable even with high turbulence levels in the outer layer; its breakdown is unexpected if the freestream turbulence intensity is less than the level of turbulence generated at the wall. Hancock[3] also provided experimental justification of log-law behavior. In the present work, the first nodal point near the wall was located between y^+ of 50 and 100, with a sensitivity study performed to show no impact of its exact placement. It was ensured that the placement of the top of the computational domain in the freestream, i.e., significantly outside the boundary layer, did not affect the results, and zero-gradient boundary conditions were applied there with the exception that $\overline{uv}$ was set equal to zero. The empirical constants in the closure are the standard values taken from the literature: $c_{\epsilon 1} = 1.45$, $c_{\epsilon 2} = 1.90$, $c_1 = 1.8$, $c_2 = 0.6$, $c_s = 0.22$, $c_\epsilon = 0.18$, $c_1' = 0.5$, $c_2' = 0.3$, and $c_w = 3.18$, as well as $\kappa = 0.41$ and $C = 5.2$ for the log-law velocity profile.

The governing parabolic equations were solved using a marching finite volume method in which they were discretized by integration over a control volume.[23] This process resulted in a coupled set of algebraic equations, which were then solved iteratively. In numerical simulations of Hancock's experiments, grid independent results were obtained using a fixed Cartesian grid with expansion in the x direction equal to twice the local momentum thickness and typically 60 geometrically expanding control volumes in the y direction. As detailed in Ref. 15, the code was validated by comparison to the analytical solution for grid turbulence, to experimental data for boundary layer flows with negligible free-stream turbulence,[24,25] and by the good agreement obtained with Rodi and Scheurer's[14] GLM predictions of mean and turbulent quantities for this flow.

IV. Comparison to Experimental Data

In numerical simulations for this flow, the influence of inlet profile specifications on downstream calculations must be considered. Shima[12] reported such a persistence for a long distance downstream. This aspect is addressed here because in Hancock's TFS experiments with turbulent profiles measured across the boundary layer (TFS2 and TFS9), the first and last measurement stations were separated by only 25 average boundary-layer thicknesses. For these two experiments, the calculations were started at an x location upstream of the first measurement station to provide a longer development length. Freestream turbulence characteristics were obtained from the analytical solution for grid turbulence, and the boundary-layer thickness was specified from an analysis of Hancock's experimental data. Details of the methodology and the results of an extensive study of the sensitivity of calculations to the specified inlet conditions for all experiments simulated are given in Ref. 15. The results are considered to be independent of upstream conditions for station 14 in run LFS4, station 8 and beyond for run TFS2, and station 10 and beyond for run TFS9. For the other four runs, results at station 8 should perhaps be viewed with some caution, but at greater x values, the effects of upstream history become minimal.

A. Local Parameters

A summary of the calculated and experimental local parameters is given in Table 1. For an LFS, the predictions are typically within 4% of experimental values. For an LFS, the calculated C_f values agree well with experimental data and are within 1% of those reported by Rodi and Scheurer[14] for runs TFS1 and TFS8. The integral parameters are also generally well predicted. With the exception of run TFS2, however, δ is overpredicted. The greatest departure of the calculations from the data is found for runs TFS3 and TFS8, where the boundary layer is initially subjected to large length scale ratios. Whereas a typical experimental error in determining δ is 5% for an LFS, it is likely larger for a TFS due to the small mean velocity gradient in the outer portion of the boundary layer. Hence, δ is a weak parameter, which is not suitable for use in evaluating turbulence models. Any significant discrepancies noted between measured and calculated L_u^∞/δ values (TFS3 and TFS8) are due to poor estimates of δ because the calculated L_u^∞ and I_∞ values are within 5% of the experimental data for all cases.

B. Mean Velocity Profiles

The calculated velocity defect profiles for a laminar freestream are generally well predicted. Excellent agreement with the velocity defect predictions of Rodi and Scheurer[14] was also obtained for both an LFS and a TFS. Also consistent with Rodi and Scheurer, log-law behavior in the near-wall region was predicted for all experimental conditions.

For a TFS, four cases were chosen to compare the effect of 1) changing I_∞ from approximately 2.5% to 4% at two nearly equal length scale ratios and 2) changing the length scale ratio from approximately 0.7 to 2.4 at two nearly equal intensities: TFS3s8 ($L_u^\infty/\delta = 2.31$ and $I_\infty = 2.24\%$); TFS2s16 ($L_u^\infty/\delta = 0.67$ and $I_\infty = 2.55\%$); TFS8s12 ($L_u^\infty/\delta = 2.53$ and $I_\infty = 3.87\%$); and TFS2s8 ($L_u^\infty/\delta = 0.71$ and $I_\infty = 3.99\%$). The velocity defect U_{def} profiles at stations TFS2s8 and TFS8s12 ($I_\infty \approx 4\%$) are shown in Fig. 1a with y nondimensionalized by the calculated δ. For reference, the experimental LFS profile is also shown. The experimental

Table 1 Summary of differences between the numerical results and the experimental data of Hancock[3]

	Average % difference from data[a]			Range	
Case	θ, δ^*	δ	C_f	L_u^∞/δ	I_∞, %
LFS3	3	8	3	——	——
LFS4	−4	4	4	——	——
TFS1	3	16	−2	1.16–0.90	5.97–2.55
TFS2	−7	−10	−3	0.77–0.67	4.82–2.55
TFS3	4	25	2	3.51–1.48	2.62–1.81
TFS8	7	28	−2	4.94–2.15	5.14–3.45
TFS9	−9	4	0	2.72–1.55	4.68–3.45

[a]Percent difference is equal to the calculated value minus the experimental value divided by the experimental value, averaged over stations not dependent on inlet specification.

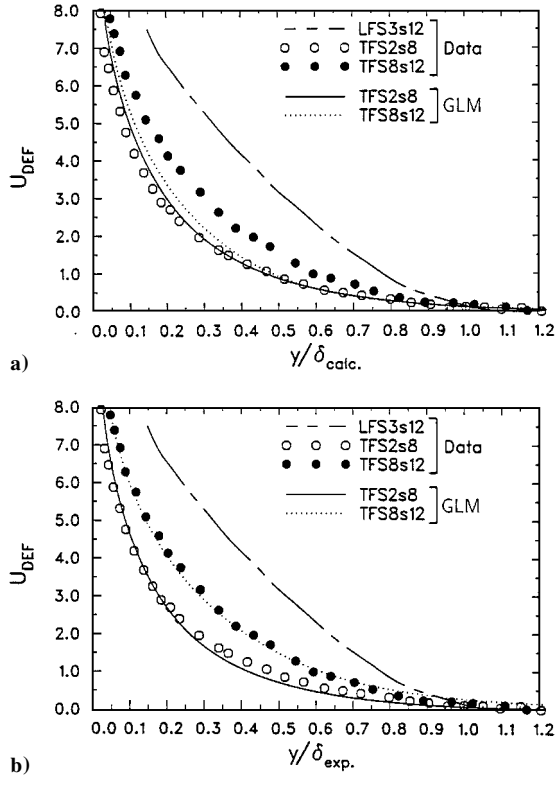

Fig. 1 Effect of length scale ratio on velocity defect at $I_\infty \approx 4\%$; cases TFS2s8 ($L_u^\infty/\delta = 0.71$) and TFS8s12 ($L_u^\infty/\delta = 2.53$): a) using δ_{calc} and b) using δ_{exp} (Ref. 3).

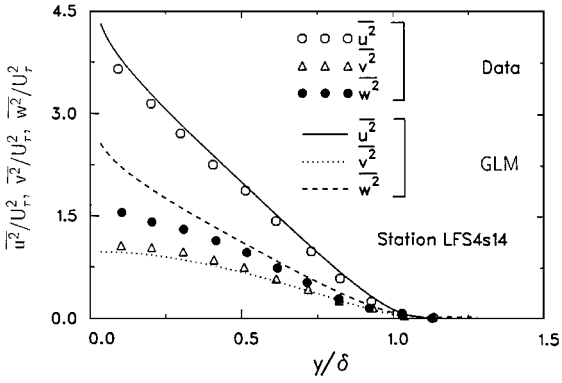

Fig. 2 Comparison of calculated normal stresses to data of Hancock[3] for an LFS.

data show a shift away from the LFS profile as L_u^∞/δ is decreased from 2.53 to 0.71. The calculated slight sensitivity to the length scale ratio is less than observed experimentally. This is due to nondimensionalizing y by the calculated δ because errors in predicting δ force the evaluation of the model to be strongly dependent on a weak parameter.[8,9,26] For these conditions, δ was underpredicted in run TFS2 by 10% and overpredicted in run TFS8 by 28%. Figure 1b clearly shows good agreement between the GLM and the data when the experimental value of δ is used in the normalization, with the models correctly capturing the experimentally observed length scale effect. The same findings hold for the velocity defect profiles at $I_\infty \approx 2.5\%$. Although not shown, the GLM also correctly predicts the effect of changing I_∞. Therefore, the effect of freestream turbulence on the mean velocity profile is well predicted. In light of these findings, the y coordinate will be nondimensionalized by the experimental δ in all subsequent comparisons to experimental data involving a TFS.

C. Turbulence Quantities

Calculations of normal stresses for an LFS are shown in Fig. 2. The $\overline{u^2}$ and $\overline{v^2}$ stresses are well predicted, although the $\overline{w^2}$ stress is

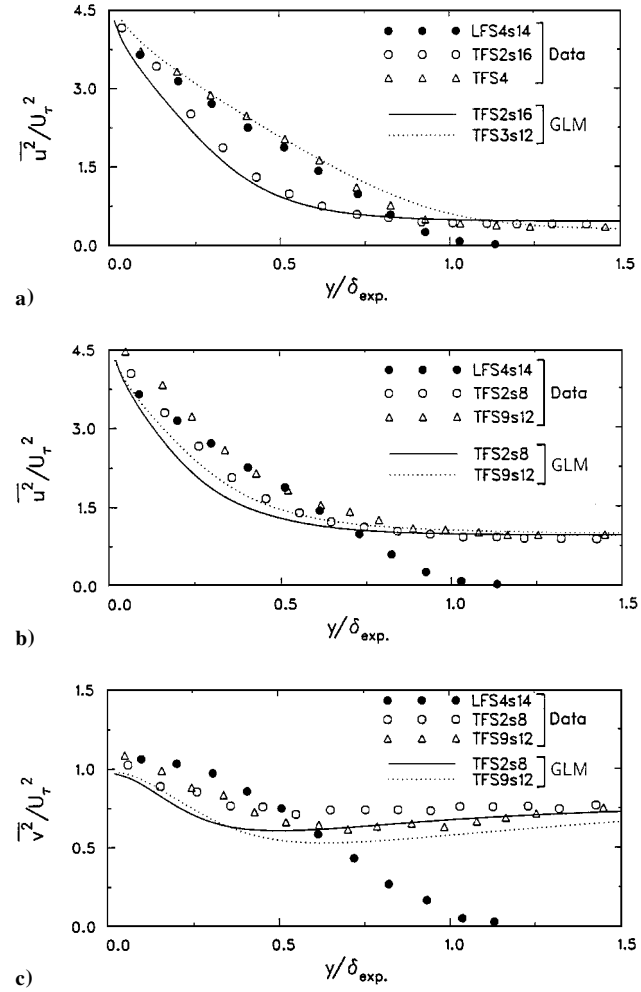

Fig. 3 Effect of length scale ratio on a) $\overline{u^2}$ at $I_\infty \approx 2.5\%$ [TFS2s16 ($L_u^\infty/\delta = 0.67$), TFS3s12 (calculation only, $L_u^\infty/\delta = 1.75$), and TFS4 (experimental data only, $L_u^\infty/\delta = 1.88$)], b) $\overline{u^2}$ at $I_\infty \approx 4\%$ [TFS2s8 ($L_u^\infty/\delta = 0.71$) and TFS9s12 ($L_u^\infty/\delta = 1.7$)], and c) $\overline{v^2}$ at $I_\infty \approx 4\%$ [TFS2s8 ($L_u^\infty/\delta = 0.71$) and TFS9s12 ($L_u^\infty/\delta = 1.7$)] (Ref. 3).

overpredicted in the inner region. Hancock's $\overline{w^2}$ profile is similar to that measured by Blair and Edwards[9] for an LFS, but below the data of Klebanoff[25] in the inner portion of the boundary layer. The effect of freestream turbulence on the turbulence stresses is assessed by comparing the effect of changing the length scale ratio at two I_∞ values. The decrease in the experimental $\overline{u^2}$ profile with a reduction in L_u^∞/δ (shown in Fig. 3a for $I_\infty \approx 2.5\%$) is due to increased mixing in the boundary layer and the reduced effect of the wall on the external turbulence. The GLM reproduces this behavior. Although not shown, similar changes in k, $\overline{v^2}$, and $\overline{uv}$ with L_u^∞/δ were also observed in the experiments and numerical predictions at this I_∞.

Calculations of $\overline{u^2}$ and $\overline{v^2}$ for a TFS ($I_\infty \approx 4\%$) are compared to data with $L_u^\infty/\delta = 1.70$ and 0.71 in Figs. 3b and 3c, respectively. Whereas the GLM predicts the same approximate degree of decrease of $\overline{u^2}$ with a reduced length scale ratio as indicated by the data, the results are approximately 15–20% below the respective measurements. Both the calculated and experimental behavior of k at I_∞ of 4% are very similar to that seen for $\overline{u^2}$ in Fig. 3b. The experimental $\overline{v^2}$ profiles for $L_u^\infty/\delta = 1.70$ are reduced from the freestream value in the outer portion of the boundary layer, whereas measurements for $L_u^\infty/\delta = 0.71$ are relatively constant throughout the outer portion of the boundary layer. In contrast, the calculations show an attenuation in the $\overline{v^2}$ levels for both cases that starts at too great a y value for the higher length scale ratio case. The calculated $\overline{v^2}$ values are below the data throughout the boundary layer at both length scale ratios. The underprediction of $\overline{v^2}$ and its attenuation at a much greater y distance than observed experimentally suggests a deficiency in the wall-reflection model in the pressure–strain term.

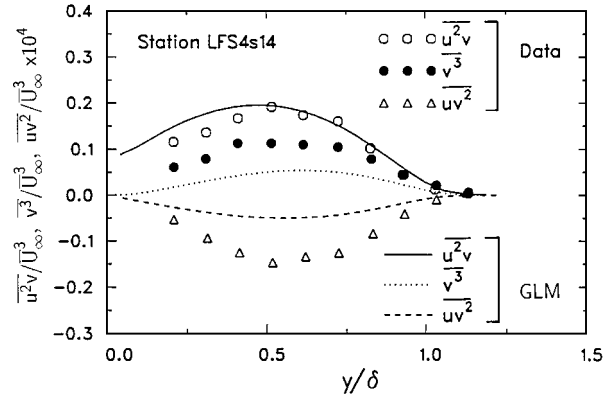

a) LFS4s14

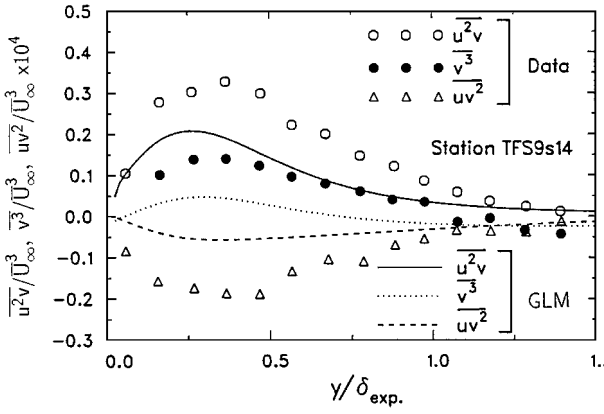

b) TFS9s14: $I_\infty \approx 4\%$ and $L_u^\infty/\delta = 1.7$

Fig. 4 Comparison of calculated third-order correlations to data of Hancock.[3]

Last, although not shown, the slight length scale ratio dependence of the $\overline{uv}$ experimental profiles is reproduced by the GLM.

Third-order correlations for an LFS are shown in Fig. 4a. The trends of $\overline{uv^2}$ and $\overline{v^3}$ are captured, but the levels are significantly underpredicted. Predictions of $\overline{u^2v}$ agree well with the data. Although not shown, the $\overline{kv}$ profile is very well predicted. Calculations (representative of the quality of predictions for a TFS) of $\overline{u^2v}$, $\overline{v^3}$, and $\overline{uv^2}$ for $I_\infty \approx 4\%$ and $L_u^\infty/\delta = 1.7$ (TFS9s14) are shown in Fig. 4b With freestream turbulence, the peak of the experimental profiles is closer to the wall than for an LFS. Although the GLM correctly predicts this shift, the data are significantly underpredicted (outside the experimental uncertainty) throughout the boundary layer. The $\overline{kv}$ data are also poorly predicted. The reduced turbulent transport of k and $\overline{u^2}$ in the outer portion of the boundary layer is consistent with the underprediction of their levels at high I_∞.

Calculations of the turbulent kinetic energy balance for both an LFS and TFS9s14 are shown in Fig. 5. The experimental observation that the production of k is in balance with the rate of dissipation outside the sublayer region is reproduced in Fig. 5a. Compared to the LFS case, the production contribution for TFS9s14 (Fig. 5b) is significantly reduced due to the smaller velocity gradient. The calculated diffusive contribution is seen to peak too close to the wall. In the outer region of the boundary layer, where the diffusion contribution is significant, the calculated diffusion levels are too low, due to the small gradients of the triple products observed in Fig. 4b. As will be shown in Sec. VI, improved predictions of the third-order correlations lead to increases in diffusion and $\overline{u^2}$ and k levels. As pointed out by Rodi and Scheurer,[14] the gradient diffusion models are not expected to be able to simulate the enhanced turbulent transport in the outer portion of the boundary layer with a TFS.

V. New Model Development

It is clear from the GLM results that improvements are needed in modeling turbulent diffusion and the effect of the wall on normal fluctuations beyond the log-law region. New formulations for these models are presented here.

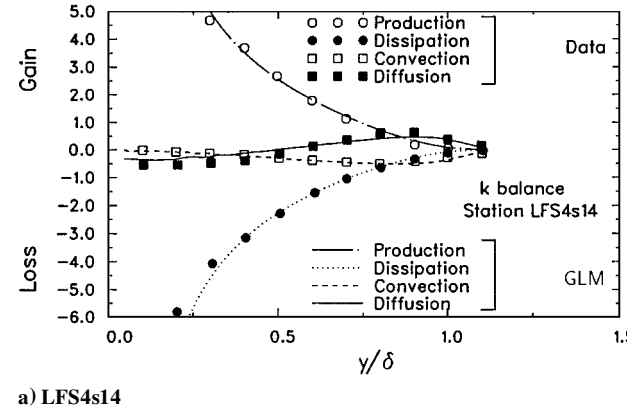

a) LFS4s14

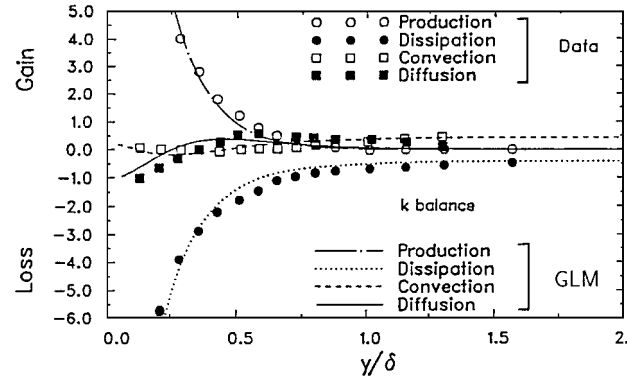

b) TFS9s14

Fig. 5 Comparison of calculated terms in the k transport equation to data of Hancock[3] (all terms multiplied by $10^4\delta/\bar{U}_\infty^3$).

A. Effect of the Wall

1. Physics of the Problem

An impermeable solid boundary affects the turbulence structure in a number of ways. Because of the no-slip condition, large mean velocity gradients exist, which are dominant factors in the production of turbulence in the boundary layer; viscosity forces all velocity components to zero close to the wall. The wall also causes the normal velocities to be suppressed, over a distance not necessarily restricted to the near-wall region, where the mean velocity gradients are large. Durbin[27,28] classifies the two roles of the wall as blocking of the normal velocity (an inviscid effect in which the velocity is brought to zero at the wall) and pressure reflection from the surface (modification of pressure fluctuations). Both these aspects are nonlocal effects, i.e., they are due to the action of the wall at a distance.

Thomas and Hancock[29] performed experiments to remove the influence of mean shear by passing a uniform, grid-generated turbulent flow with velocity $\bar{U}_\infty$ over a wall also moving at $\bar{U}_\infty$. The $\overline{v^2}$ suppression, therefore, could be directly attributed to the blocking effect already discussed. The experiments were performed using two grids with measurements taken at three streamwise locations, where I_∞ was 4.25, 5.25, and 7.75%. The nondimensional $\overline{v^2}$ profiles ($\overline{v^{2^*}} = \overline{v^2}/\overline{v_\infty^2}$) vs $y^* = y/L_{ue}$ are seen in Fig. 6 to have geometrically similar behavior and follow the empirical correlation $\overline{v^{2^*}} = 1 - \exp(-2.97y^*)$. Although not shown, the nondimensional $\overline{u^2}$ values increase as the wall is approached, whereas $\overline{w^2}$ remains relatively constant; similarity was seen only for $\overline{v^2}$.

A similar plot of Hancock's data (with a stationary wall) is shown in Fig. 7. Similarity is observed for data outside the boundary-layer edge (indicated by filled symbols). Both the wall-blocking and pressure-reflection effects of the wall are present in this flow. The increase in $\overline{v^{2^*}}$ as $y^* \to 0$ is due to shear-produced turbulence in the boundary layer. The data of Blair and Edwards[9] ($I_\infty \approx 3\%$) display similar behavior.

2. Similarity Equation for $\overline{v^2}$

It has been demonstrated that regardless of the near-wall structure, the wall attenuates the $\overline{v^2}$ component in an apparent universal

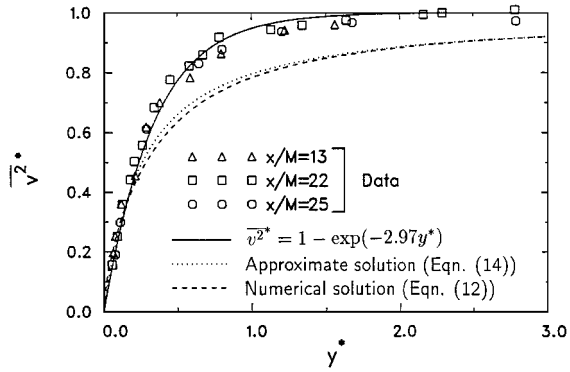

Fig. 6 Comparison of calculated $\overline{v^2}^*$ from similarity solution using Gibson and Launder's[13] wall-reflection term to the zero-mean shear data of Thomas and Hancock.[29]

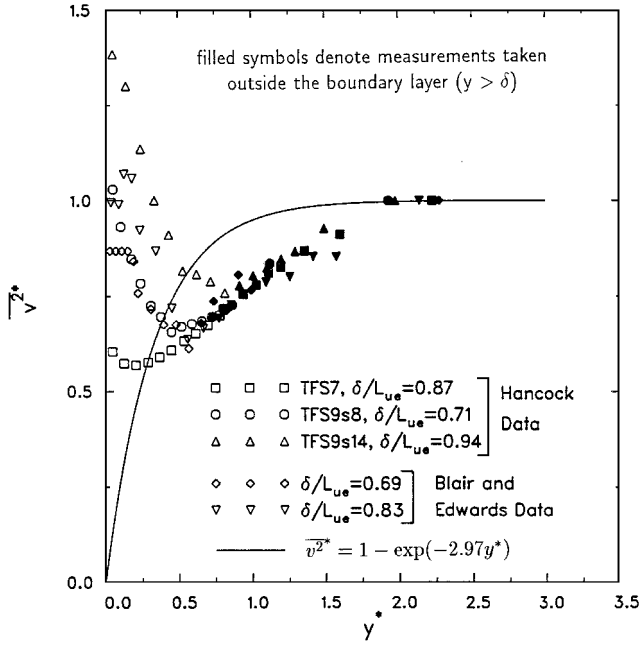

Fig. 7 Variation of $\overline{v^2}^*$ data for the boundary-layer flows of Hancock[3] and Blair and Edwards.[9]

manner. Therefore, any model should be able to be cast in a self-similar form and accurately predict the data. Durbin[27] points out that in a single-point closure, both the wall effects (blocking and pressure reflection) should be represented. A similarity equation for $\overline{v^2}$ will now be derived for the shear-free flow to understand the failure of GLM to predict the $\overline{v^2}$ profile (refer to Fig. 3c). The methodology followed in this derivation may be used as a basis to assess any turbulence closure's ability to model the effect of the wall.

A simplified form of the $\overline{v^2}$ equation for the shear-free flow is obtained by considering a uniform velocity field $(\bar{U}, \bar{V}, \bar{W}) = (\bar{U}_\infty, 0, 0)$. It is also assumed that k and ϵ are independent of y, which is reasonable except possibly in the near-wall region. Hunt[30] reports that ϵ is approximately constant with y. Measurements of k for two of Thomas and Hancock's[29] three cases show that they are within approximately 3% of k_∞ for y^* greater than 0.2, whereas for the third case k is within approximately 6% of k_∞ for y^* greater than 0.5. With these assumptions, the $\overline{v^2}$ equation approximates to

$$\frac{\bar{U}_\infty}{\epsilon}\frac{\overline{v_\infty^2}}{\partial x}\frac{\partial \overline{v^2}^*}{\partial x} + \frac{2}{3}(c_1 - 1)\overline{v^2}^* = \frac{2}{3}(c_1 - 1) + c_s\alpha_2^2\left(\frac{k^{\frac{3}{2}}}{\epsilon}\right)^2 \times \frac{1}{L_{ue}^2}\frac{\partial}{\partial y^*}\left(\overline{v^2}^*\frac{\partial \overline{v^2}^*}{\partial y^*}\right) - \frac{W}{\epsilon} \tag{10}$$

where $\alpha_2 = \overline{v_\infty^2}/k$ and the W term accounts for the wall effect on the attenuation of $\overline{v^2}$. A relationship between L_{ue} and $k^{3/2}/\epsilon$ is derived by applying the modeled form of the $\overline{u^2}$ conservation equation in the freestream and the definition of L_u^∞ [Eq. (1)]:

$$\frac{k^{\frac{3}{2}}}{\epsilon} = mL_{ue}, \qquad m = \left(\frac{2/3 + c_1(\alpha_1 - 2/3)}{\alpha_1^{3/2}}\right)p_r \tag{11}$$

where $p_r = L_u^\infty/L_{ue}$ and $\alpha_1 = \overline{u_\infty^2}/k$. For $0.65 < \alpha_1 < 1.0$, $m = 1.225p_r$ (to within 4%). Therefore, with $k^{3/2}/\epsilon = 1.225p_rL_{ue}$, and imposing similarity, i.e., gradients of $\overline{v^2}^*$ with respect to x are zero, the governing equation for $\overline{v^2}^*$ becomes

$$c_s'\frac{\partial}{\partial y^*}\left(\overline{v^2}^*\frac{\partial \overline{v^2}^*}{\partial y^*}\right) - \frac{2}{3}(c_1 - 1)\overline{v^2}^* = -\frac{2}{3}(c_1 - 1) + \frac{W}{\epsilon} \tag{12}$$

where $c_s' = 1.5c_s\alpha_2^2p_r^2$. The $\overline{v^2}^*$ profile may, therefore, be determined for a given form of W. If diffusion is neglected, then the solution to Eq. (12) is

$$\overline{v^2}^* = 1 - \frac{3}{2}\frac{W}{(c_1 - 1)\epsilon} \tag{13}$$

The Gibson and Launder[13] form of W is $2c_1'\overline{v^2}f(\epsilon/k)$, where $f = k^{3/2}/c_w\epsilon y$. Substituting for W into Eq. (13) with $c_1' = 0.5$ gives

$$\overline{v^2}^* = \frac{1}{1 + (A_{\mathrm{GL}})/y^*}, \qquad A_{\mathrm{GL}} = \frac{3\alpha_2 m}{2c_w(c_1 - 1)} \tag{14}$$

An analysis of Thomas and Hancock's[29] data gives $p_r = 0.573$, an average $\alpha_2 = 0.62$, and, hence, A_{GL} in Eq. (14) equals 0.257. The values of $\overline{v^2}^*$ obtained from the full numerical solution of Eq. (12) and from the approximate solution given by Eq. (14) are compared to experimental data in Fig. 6. Because the retention of the diffusion term does not significantly alter the calculated $\overline{v^2}^*$ values, the approximate solution given by Eq. (14) is justified. In addition, it is apparent that the attenuation of $\overline{v^2}^*$ by the wall as modeled by Gibson and Launder[13] is overestimated. This deficiency is because only near-wall modifications of turbulent stresses in regions of high mean shear were considered when the model was developed; the observed influence of the wall on the region of small or no mean velocity gradient is not accounted for.

3. *Alternative Wall-Reflection Formulation*

Model formulations would ideally not require a wall-reflection term. Significant effort is reported in the modeling community to minimize or remove the contribution of the wall-reflection term. One example of such work is that of Durbin,[27,28] in which the nonlocal effect of the wall in modifying the v fluctuations is treated by introducing elliptic relaxation of the pressure–velocity and dissipation terms. It should be noted, however, that Durbin's modeling was tailored to the problem of near-wall flows (within the log-law region). The usefulness of his model for the present problem is not clear. The current work is concerned with calculations outside the log-law region; the elliptic relaxation is not appreciable far from the wall, where Durbin's models reduce to a standard quasihomogeneous form. Because the wall-reflection formulation is still a basis for many low and high Reynolds number closures, and alternative formulations have been developed for specific applications, e.g., Craft and Launder,[31] modifications to it will be pursued here.

The new wall-reflection formulation considers behavior in both the similarity, i.e., outside the boundary layer, and the log-law regions; the GLM considered near-wall behavior only. The general form of the GLM is maintained [refer to Eq. (8)], but a new length scale function f^* is introduced. The wall-reflection term for the $\overline{v^2}$ equation for the shear-free flow is

$$W = 2c_1'\overline{v^2}f^*\epsilon/k \tag{15}$$

Substitution of Eq. (15) into Eq. (13) yields

$$f^* = C^*P^*\left(1 - \overline{v^2}^*\right)/\overline{v^2}^* \tag{16}$$

where $P^* = (c_1 - 1)/(3c_1'\alpha_2)$. C^* is determined by specifying the value of f^* at the first nodal point in the log-law region to equal unity. The empirical relationship $\overline{v^2}^* = 1 - e^{by^*}$, shown earlier to give a good approximation to the experimental data, is used to derive the functional form of f^*. In terms of calculated variables for Hancock's

flow ($\alpha_2 = 0.65$ and $p_r = 1.59$), $y^* = 1.96y/(k^{3/2}/\epsilon) = 0.252/\kappa$. Thus, the final form of f^* is

$$f^* = \frac{(1 - e^{0.615b})e^{by^*}}{e^{0.615b}(1 - e^{by^*})}, \qquad y^* = 1.96\left(\frac{y}{k^{1.5}/\epsilon}\right) \tag{17}$$

Note that $\overline{v^2}$ itself does not appear in the formulation of f^*. It will be shown in Sec. VI that excellent predictions of $\overline{v^2}$ are obtained when Eq. (17) is used in calculations.

B. Turbulent Diffusion

1. *Assessment of Existing Models*

Because of poor predictions of the third-order correlations and the increased role of turbulent diffusion with freestream turbulence, an investigation of models for $\overline{u_i u_j u_k}$ was performed. A review of the literature identified three general categories of models: modeling via the $\overline{u_i u_j u_k}$ conservation equation, gradient diffusion models, and structural models based on coherent motions. Based on analysis and preliminary testing (see Ref. 15 for details), the latter two approaches were not considered further (with the exception of the gradient diffusion model of Daly and Harlow[20]). For example, the coherent structure model of Nagano and Tagawa[32] gave poor predictions of $\overline{u^2 v}$ with freestream turbulence.

The following $\overline{u_i u_j u_k}$ conservation equation formulations were considered: Hanjalic and Launder,[33] Andre et al.,[34] Dekeyser and Launder,[35] Amano and Chai,[36] and Amano et al.[37] These models were developed considering different flows and differ by the assumptions made in modeling the terms and in the values of the constants. A discussion of the exact and modeled forms of the $\overline{u_i u_j u_k}$ equations will be presented in the next section in the derivation of a new formulation.

The following findings were obtained from simulations of Hancock's LFS case LFS4s14 and free-stream turbulence cases, employing the various diffusion models in the solution of the governing equations. (Note that the convective terms in Amano's models were not included in the present work to render all expressions algebraic.)

1) Some models (Dekeyser and Launder[35] and Amano and Chai[36]) gave poor predictions for an LFS.

2) Calculations of $\overline{kv}$ and $\overline{u^2 v}$ obtained with the Daly and Harlow[20] model are quantitatively similar to those obtained with the best of the transport equation-based models, Andre et al.[34] The latter model gives overall better predictions of $\overline{v^3}$ and $\overline{uv^2}$.

3) The Daly and Harlow[20] and Andre et al.[34] models respond correctly to experimentally observed changes in the length scale ratio but not to changes in intensity.

4) As the freestream becomes increasingly turbulent, none of the models considered gave good predictions of the triple products.

2. *Development of Improved Turbulent Diffusion Models*

Because of the demonstrated deficiencies in the existing diffusion models, two new diffusion models were formulated to seek improved predictions. In the first formulation, a modification to the conventional gradient diffusion formulation is proposed by directly accounting for the increased transport with increasing freestream turbulence intensity. The diffusion constant c_s in Eq. (5) is multiplied by the empirical function $g = 1 + cI_\infty^d$, where the constants c and d are chosen based on comparisons with data.

The second model proposed is based on the formulation of Andre et al.[34] (unless otherwise noted), the transport equation-based model that gave the best predictions of Hancock's data. The exact form of the $\overline{u_i u_j u_k}$ equation is

$$\underbrace{\frac{\mathrm{D}\overline{u_i u_j u_k}}{\mathrm{D}t}}_{C_{ijk}} = \underbrace{-\frac{\partial}{\partial x_l}\left(\overline{u_i u_j u_k u_l} + \frac{\overline{p u_j u_k}}{\rho}\delta_{il} + \frac{\overline{p u_i u_k}}{\rho}\delta_{jl} + \frac{\overline{p u_i u_j}}{\rho}\delta_{kl} - \nu\frac{\partial}{\partial x_l}\overline{u_i u_j u_k}\right)}_{D_{ijk}} + \underbrace{\left(\overline{u_i u_j}\frac{\partial \overline{u_k u_l}}{\partial x_l} + \overline{u_k u_i}\frac{\partial \overline{u_j u_l}}{\partial x_l} + \overline{u_j u_k}\frac{\partial \overline{u_i u_l}}{\partial x_l}\right)}_{P_{ijk,1}}$$

$$\underbrace{-\left(\overline{u_i u_j u_l}\frac{\partial \bar{U}_k}{\partial x_l} + \overline{u_k u_i u_l}\frac{\partial \bar{U}_j}{\partial x_l} + \overline{u_j u_k u_l}\frac{\partial \bar{U}_i}{\partial x_l}\right)}_{P_{ijk,2}} + \underbrace{\overline{\frac{p}{\rho}\left(\frac{\partial u_i u_j}{\partial x_k} + \frac{\partial u_k u_i}{\partial x_j} + \frac{\partial u_j u_k}{\partial x_i}\right)}}_{\phi_{ijk}} - \underbrace{2\nu\left(\overline{\frac{\partial u_k u_i}{\partial x_l}\frac{\partial u_j}{\partial x_l}} + \overline{\frac{\partial u_j u_k}{\partial x_l}\frac{\partial u_i}{\partial x_l}} + \overline{\frac{\partial u_i u_j}{\partial x_l}\frac{\partial u_k}{\partial x_l}}\right)}_{\epsilon_{ijk}} \tag{18}$$

where the terms are convection, diffusion, production by turbulent quantities only, production by mean velocity gradients, pressure interactions, and dissipation, respectively.

Convection is neglected and the dissipation term is omitted on the basis that, at high Re_t, viscous terms are negligible or local isotropy renders the terms equal to zero. No modeling is required for the production terms. Diffusion by pressure fluctuations is not considered separately and molecular diffusion is negligible. The fourth-order product $\overline{u_i u_j u_k u_l}$ is simplified by applying the quasinormal approximation

$$\overline{u_i u_j u_k u_l} = \overline{u_i u_j}\,\overline{u_k u_l} + \overline{u_i u_k}\,\overline{u_j u_l} + \overline{u_i u_l}\,\overline{u_j u_k} \tag{19}$$

The diffusion term may then be combined with $P_{ijk,1}$ to give DP_{ijk}

$$DP_{ijk} = D_{ijk} + P_{ijk,1} = -\left(\overline{u_k u_l}\frac{\partial \overline{u_i u_j}}{\partial x_l} + \overline{u_j u_l}\frac{\partial \overline{u_i u_k}}{\partial x_l} + \overline{u_i u_l}\frac{\partial \overline{u_j u_k}}{\partial x_l}\right) \tag{20}$$

Analogous to the derivation and modeling of the pressure–strain term in the $\overline{u_i u_j}$ equation, the pressure-interaction term is expressed in terms of contributions from both volume and surface integrals

$$\phi_{ijk} = \phi_{ijk,1} + \phi_{ijk,2} + \phi_{ijk,w} \tag{21}$$

corresponding to interactions between fluctuating quantities only, interactions with mean velocity gradients, and the influence of a solid boundary, respectively. The concept of return to isotropy is applied to $\phi_{ijk,1}$ by relating the correlation to the triple product itself and introducing the turbulent timescale T_s (typically taken as k/ϵ):

$$\phi_{ijk,1} = -\frac{\overline{u_i u_j u_k}}{c_{\phi 1} T_s} \tag{22}$$

The following two aspects differ from the treatment of Andre et al.[34] First, $\phi_{ijk,2}$ is retained following Dekeyser and Launder's[35] reasoning that if $P_{ijk,2}$ is significant, then so should $\phi_{ijk,2}$ be significant. The term is modeled by relating it to $P_{ijk,2}$

$$\phi_{ijk,2} = -c_{\phi 2} P_{ijk,2} \tag{23}$$

Second, it is proposed here to relate $\phi_{ijk,w}$ to $\overline{u_i u_j u_k}$ and the length scale function f^*. Therefore, the expression for ϕ_{ijk} is

$$\phi_{ijk} = -\left(\frac{1 + f^*}{c_{\phi 1}}\right)\frac{\overline{u_i u_j u_k}}{k/\epsilon} - c_{\phi 2} P_{ijk,2} \tag{24}$$

This $\phi_{ijk,w}$ model may also be interpreted as introducing a modified timescale $T_s = k/[(1+f^*)\epsilon]$, an alternate approach used by Amano and Chai[36] and Amano et al.[37] to represent wall effects. Thus, the $\overline{u_i u_j u_k}$ model becomes

$$\overline{u_i u_j u_k} = \left[c_{\phi 1} g/(1 + f^*)\right](k/\epsilon)[DP_{ijk} + (1 - c_{\phi 2})P_{ijk,2}] \tag{25}$$

The empirical function $g = 1 + cI_\infty^d$ is introduced to effectively modify $c_{\phi 1}$, where the constants c and d are chosen based on experimental data. Note that for thin shear layer flows, such as that considered here, many of the terms associated with mean shear (in $P_{ijk,2}$) are small.

In summary, the formulation in Eq. (25) is based on applying modeling assumptions to the exact conservation equation for the third-order correlation. The modeling of the terms is consistent with

Table 2 Differences between the GSM, TSM, and GLM

Quantity	GLM	GSM	TSM
$\overline{u_i u_j u_k}$	$-c_s \frac{k}{\epsilon} \overline{u_k u_l} \frac{\partial \overline{u_i u_j}}{\partial x_l}$	$-c_s \frac{k}{\epsilon} g \overline{u_k u_l} \frac{\partial \overline{u_i u_j}}{\partial x_l}$	$\frac{c_{\phi 1} g}{1+f^*} \frac{k}{\epsilon} [D P_{ijk} + (1-c_{\phi 2}) P_{ijk,2}]$
		$g = 1 + c(I_\infty)^d$	$g = 1 + c(I_\infty)^d$
Length scale	$f = \frac{k^{1.5}}{c_w \epsilon y}$	$f^* = 1.22\left(\frac{e^{by^*}}{1-e^{by^*}}\right)$	$f^* = 1.22\left(\frac{e^{by^*}}{1-e^{by^*}}\right)$
Function [Eq. (8)]		$y^* = \left(1.96 \frac{y}{k^{1.5}/\epsilon}\right)$	$y^* = \left(1.96 \frac{y}{k^{1.5}/\epsilon}\right)$
c_s	0.22	0.20	——
$c_{\phi 1}$	——	——	0.11
$c_{\phi 2}$	——	——	0.6
c_ϵ	0.18	0.18	0.16
b	——	−1.3	−1.3
c, d	——	0.045, 2	0.07, 2

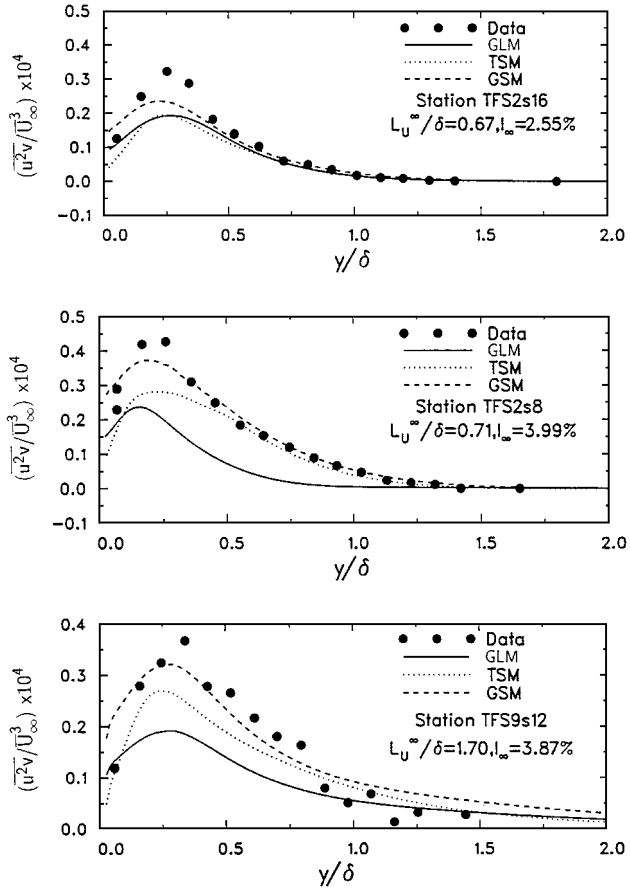

Fig. 8 Predictions of $\overline{u^2 v}$ using the GLM, GSM, and TSM for TFS cases TFS2s16, TFS2s8, and TFS9s12 (Ref. 3).

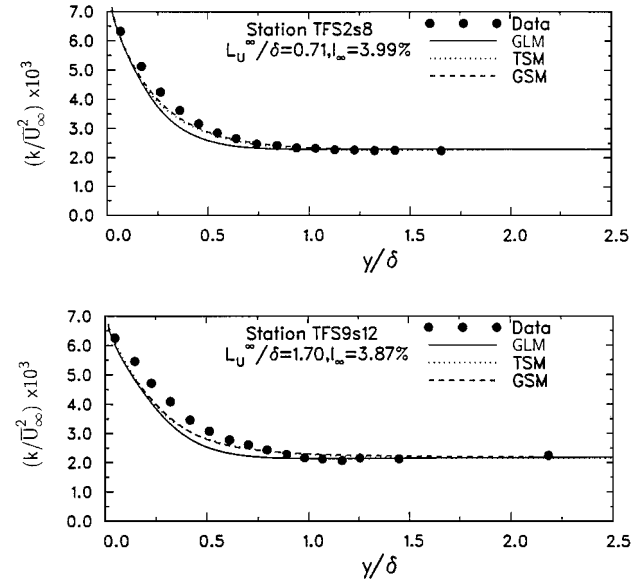

Fig. 9 Predictions of k using the GLM, GSM, and TSM for TFS cases TFS2s8 and TFS9s12 (Ref. 3).

the approach taken by many other workers who have applied their models to a wide range of flows. The model proposed in the present work has only been tested for boundary layer flows with both an LFS and a TFS. Further testing is required before the proposed model is applied outside its validated range.

VI. Evaluation of the New Formulations

Calculations with two new Reynolds stress model formulations are compared to those obtained with the GLM in this section. Both new formulations use the new wall-reflection treatment presented in Sec. V. The formulations differ by the turbulent diffusion treatment: one formulation employs the modified gradient diffusion model (denoted GSM), and the other is based on the $\overline{u_i u_j u_k}$ transport equation [Eq. (25)] (denoted TSM). The differences between the GLM and the new formulations are given in Table 2. The constant values for the new formulations were chosen to give reasonable predictions of variables for both an LFS and a TFS. For an LFS, the models provide acceptable agreement with the data of Klebanoff[25] and Hancock.[3]

The comparisons between the model predictions and experimental data shown here are limited to a few selected variables with freestream turbulence. Calculations are compared to Hancock's data for the following three cases to evaluate the effect of changing both the intensity and the length scale ratio: 1) TFS2s16: $I_\infty = 2.55\%$ and $L_u^\infty/\delta = 0.67$; 2) TFS2s8: $I_\infty = 3.99\%$ and $L_u^\infty/\delta = 0.71$; and 3) TFS9s12: $I_\infty = 3.87\%$ and $L_u^\infty/\delta = 1.70$. Although not shown, it was demonstrated that the mean velocity predictions, in particular the near-wall behavior, are similar using the three models (as was also found for the LFS cases). Calculations of the integral parameters θ and δ^* as well as C_f show differences of less than 2% between new and old model predictions.

General conclusions as to the improvement in the predictions of the third-order correlations are demonstrated by the $\overline{u^2 v}$ calculation shown in Fig. 8. Both new models give better predictions at higher intensities, with the GSM better. At low intensity, calculations with all three models are similar in the outer portion of the boundary layer, where a reasonable prediction of the data is found. Predictions of $\overline{kv}$ (not shown here) show similar improvements as found for $\overline{u^2 v}$.

Predictions of k using the three models are shown in Fig. 9 for two cases only; $\overline{w^2}$ was not reported at station TFS2s16. The GSM and TSM give similar predictions and are within expected experimental uncertainly. The higher k levels calculated with the new models are explained as largely due to the improved predictions of the third-order correlations and their impact on the contribution of diffusion to the balance. Figure 10 shows clearly that the $\overline{v^2}$ data are much

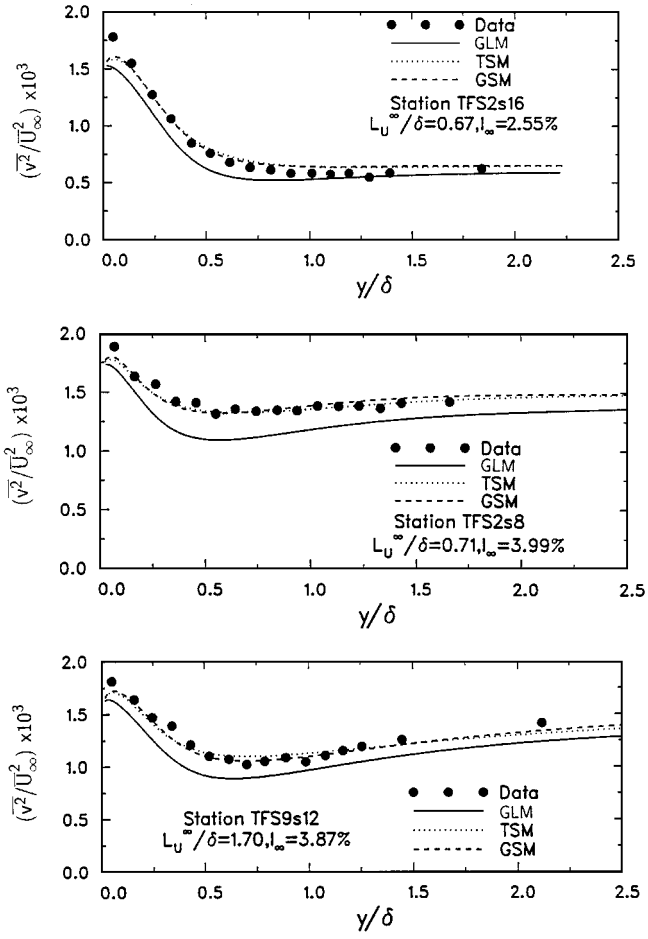

Fig. 10 Predictions of $\overline{v^2}$ using the GLM, GSM, and TSM for TFS cases TFS2s16, TFS2s8, and TFS9s12 (Ref. 3).

better predicted with both new formulations than with the GLM, a result of the new wall-reflection model. The calculated stress levels also return to the experimental freestream values much nearer to the wall with the new models. Although not shown, the impact of the new formulations on $\overline{u^2}$ predictions is similar to that found for k. All models produce similar $\overline{uv}$ results in the inner portion of the boundary layer but the new formulations give slightly greater values in the outer region due to larger predicted values of $\overline{uv^2}$.

VII. Conclusions

A study of high Reynolds number closures to predict the effect of freestream turbulence on a boundary layer has been presented. A procedure was developed, which is recommended for any future testing of models for this flow. Key aspects include the choice of experiments to isolate the effects of changes in length scale ratio and freestream turbulence intensity, and the requirements to predict self-similarity of $\overline{v^2}$ for a zero mean shear flow. The integral parameters and friction coefficient are well predicted by the widely used GLM. Experimentally observed trends in turbulent and mean profiles as a function of the freestream turbulence intensity and the length scale ratio are also generally well predicted by the GLM. The GLM, however, does not properly account for the effect of the wall in attenuating the fluctuations normal to the solid surface. In addition, the third-order correlations and the turbulent diffusion contribution are underpredicted. These two aspects were identified for further investigation.

Based on the experimental observation of similarity for $\overline{v^2}$ in both the zero mean shear and conventional boundary-layer flows, a new formulation of the wall-reflection term has been obtained, which considers both near-wall and far-field behavior. Also, two turbulent diffusion models have been proposed, one based on a modified gradient diffusion approximation (GSM) and the other on the conservation equation for $\overline{u_i u_j u_k}$ (TSM). Both the new wall-reflection and diffusion terms have been implemented into a Reynolds stress model. It is demonstrated that the new models result in improved predictions of $\overline{v^2}$, $\overline{u^2}$, and k and the triple products, as well as other variables of interest, with the exception of δ and $\overline{uv}$ at the boundary-layer edge at higher intensities. Given its relative simplicity and accuracy, the GSM is recommended.

Acknowledgments

Funding was provided under grants from the Natural Sciences and Engineering Research Council of Canada and the Manufacturing Research Corporation of Ontario.

References

[1]Blair, M. F., "Influence of Free-Stream Turbulence on Turbulent Boundary Layer Heat Transfer and Mean Profile Development, Part I: Experimental Data, and Part II: Analysis of Results," *Journal of Heat Transfer*, Vol. 105, Feb. 1983, pp. 33–47.

[2]Castro, I. P., "Effects of Free Stream Turbulence on Low Reynolds Number Boundary Layers," *Journal of Fluids Engineering*, Vol. 106, Sept. 1984, pp. 298–306.

[3]Hancock, P. E., "The Effect of Free-Stream Turbulence on Turbulent Boundary Layers," Ph.D. Thesis, Dept. of Aeronautics, Imperial College, London, July 1980.

[4]Hancock, P. E., and Bradshaw, P., "The Effect of Free-Stream Turbulence on Turbulent Boundary Layers," *Journal of Fluids Engineering*, Vol. 105, Sept. 1983, pp. 284–289.

[5]Hancock, P. E., and Bradshaw, P., "Turbulence Structure of a Boundary Layer Beneath a Turbulent Free Stream," *Journal of Fluid Mechanics*, Vol. 205, Aug. 1989, pp. 45–76.

[6]Baskaran, V., Abdellatif, O. E., and Bradshaw, P., "Effects of Free-Stream Turbulence on Turbulent Boundary Layers with Convective Heat Transfer," *Proceedings of the Seventh Symposium on Turbulent Shear Flows*, Stanford Univ., Stanford, CA, 1989, pp. 20.1.1–20.1.6.

[7]Hoffmann, J. A., and Mohammadi, K., "Velocity Profiles for Turbulent Boundary Layers Under Free-Stream Turbulence," *Journal of Fluids Engineering*, Vol. 113, Sept. 1991, pp. 399–404.

[8]McDonald, H., and Kreskovsky, J. P., "Effect of Free Stream Turbulence on the Turbulent Boundary Layer," *International Journal of Heat and Mass Transfer*, Vol. 17, July 1974, pp. 705–716.

[9]Blair, M. F., and Edwards, D. E., "The Effects of Free-Stream Turbulence on the Turbulence Structure and Heat Transfer in Zero Pressure Gradient Boundary Layers," United Technologies Research Center, TR R82-915634-2, Hartford, CT, Nov. 1982.

[10]Bradshaw, P., "Effect of Free-Stream Turbulence on Boundary Layers," *1980–81 AFOSR-HTTM Stanford Conference on Complex Turbulent Flows*, Vol. 1, Thermosciences Div., Mechanical Engineering Dept., Stanford Univ., Stanford, CA, 1980, pp. 86–93.

[11]Savill, A. M., "Algebraic and Reynolds Stress Modeling of Manipulated Boundary Layers Including Effect of Free-Stream Turbulence," *Proceedings of the Royal Aeronautical Society International Conference on Turbulent Drag Reduction by Passive Means* (London), Vol. 1, 1987, pp. 89–143.

[12]Shima, N., "Prediction of Turbulent Boundary Layers with a Second-Moment Closure: Part I—Effects of Periodic Pressure Gradient, Wall Transpiration and Free-Stream Turbulence," *Journal of Fluids Engineering*, Vol. 115, March 1993, pp. 56–63.

[13]Gibson, M. M., and Launder, B. E., "Ground Effects on Pressure Fluctuations in the Atmospheric Boundary Layer," *Journal of Fluid Mechanics*, Vol. 86, Pt. 3, 1978, pp. 491–511.

[14]Rodi, W., and Scheurer, G., "Calculation of Turbulent Boundary Layers Under the Effect of Free Stream Turbulence," *Proceedings of the Fifth Symposium on Turbulent Shear Flows*, Cornell Univ., Ithaca, NY, 1985, pp. 2.19–2.25.

[15]Mackinnon, J. C., "A Critical Evaluation of the Reynolds Stress Turbulence Closure for the Flow of a Turbulent Free-Stream over a Turbulent Boundary Layer," Ph.D. Thesis, Dept. of Mechanical Engineering, Univ. of Waterloo, Waterloo, ON, Canada, 1992.

[16]Charnay, G., Mathieu, J., and Comte-Bellot, G., "Response of a Turbulent Boundary Layer to Random Fluctuations in the External Stream," *Physics of Fluids*, Vol. 19, No. 9, 1976, pp. 1261–1272.

[17]de Brederode, V., and Bradshaw, P., "Influence of the Side Walls on the Turbulent Center-Plane Boundary-Layer in a Square Duct," *Journal of Fluids Engineering*, Vol. 100, March 1978, pp. 91–96.

[18]Johnston, J. P., and Flack, K. A., "Review—Advances in Three-Dimensional Turbulent Boundary Layers with Emphasis on the Wall-Layer Regions," *Journal of Fluids Engineering*, Vol. 118, June 1996, pp. 219–232.

[19]Jakirlic, S., and Hanjalic, K., "A Second-Moment Closure for Non-Equilibrium and Separating High- and Low-Re-Number Flows," *Proceedings of the Tenth Symposium on Turbulent Shear Flows*, 1995, pp. 23-25–23-30.

[20]Daly, B. J., and Harlow, F. H., "Transport Equations in Turbulence," *Physics of Fluids*, Vol. 13, 1970, pp. 2634–2649.

[21]Launder, B. E., Reece, G. J., and Rodi, W., "Progress in the Development of a Reynolds-Stress Turbulence Closure," *Journal of Fluid Mechanics*, Vol. 68, Pt. 3, 1975, pp. 537–566.

[22]Bradshaw, P., "Effect of Free-Stream Turbulence on Turbulent Shear Layers," Imperial College, Aero. Rept. 74-10, London, Oct. 1974.

[23]Patankar, S. V., *Numerical Heat Transfer and Fluid Flow*, Hemisphere, Washington, DC, 1980, pp. 25–111.

[24]Wieghardt, K., and Tillmann, W., "On the Turbulent Friction Layer for Rising Pressure," NACA TM-1314, 1951.

[25]Klebanoff, P. S., "Characteristics of Turbulence in a Boundary Layer with Zero Pressure Gradient," NACA Rept. 1247, 1955.

[26]Launder, B. E., "Computors Report," *1980-81 AFOSR-HTTM Stanford Conference on Complex Turbulent Flows*, Vol. 3, Thermosciences Div., Mechanical Engineering Dept., Stanford Univ., Stanford, CA, 1981, pp. 1390–1407.

[27]Durbin, P., "Near-Wall Turbulence Closure Modeling Without Damping Functions," *Theoretical and Computational Fluid Dynamics*, Vol. 3, 1991, pp. 1–13.

[28]Durbin, P., "A Reynolds Stress Model for Near-Wall Turbulence," *Journal of Fluid Mechanics*, Vol. 249, April 1993, pp. 465–498.

[29]Thomas, N. H., and Hancock, P. E., "Grid Turbulence Near a Moving Wall," *Journal of Fluid Mechanics*, Vol. 82, Pt. 3, 1977, pp. 481–496.

[30]Hunt, J. C. R., "Turbulence Structure in Thermal Convection and Shear-Free Boundary Layers," *Journal of Fluid Mechanics*, Vol. 138, June 1984, pp. 161–184.

[31]Craft, T. J., and Launder, B. E., "New Wall-Reflection Model Applied to the Turbulent Impinging Jet," *AIAA Journal*, Vol. 30, No. 12, 1992, pp. 2970–2972.

[32]Nagano, Y., and Tagawa, M., "Statistical Characteristics of Wall Turbulence with a Passive Scalar," *Journal of Fluid Mechanics*, Vol. 196, Nov. 1988, pp. 157–185.

[33]Hanjalic, K., and Launder, B. E., "A Reynolds Stress Model of Turbulence and Its Application to Thin Shear Flows," *Journal of Fluid Mechanics*, Vol. 52, Pt. 4, 1972, pp. 609–638.

[34]Andre, J. C., De Moor, G., Lacarrere, P., Therry, G., and du Vachat, R., "The Clipping Approximation for Inhomogeneous Turbulence," *Proceedings of the First Symposium on Turbulent Shear Flows*, 1977, pp. 4.39–4.46.

[35]Dekeyser, I., and Launder, B. E., "A Comparison of Triple-Moment Temperature–Velocity Correlations in the Asymmetric Heated Jet with Alternative Closure Models," *Proceedings of the Fourth Symposium on Turbulent Shear Flows*, 1983, pp. 14.1–14.8.

[36]Amano, R. S., and Chai, J. C., "Transport Models of the Turbulent Velocity–Temperature Products for Computations of Recirculating Flows," *Numerical Heat Transfer*, Vol. 14, 1988, pp. 75–95.

[37]Amano, R. S., Goel, P., and Chai, J. C., "Turbulence Energy and Diffusion Transport of Third Moments in a Separating and Reattaching Flow," *AIAA Journal*, Vol. 26, No. 3, 1988, pp. 273–282.

C. G. Speziale
Associate Editor